ANALYSIS OF EPIDEMIC PROCESSES OVER NETWORKS: ASYMPTOMATIC CASES AND THE SAIRS MODEL

BY

XIAOQI BI

THESIS

Submitted in partial fulfillment of the requirements
for the degree of Master of Science in Industrial Engineering
with a concentration in Advanced Analytics in IESE
in the Graduate College of the
University of Illinois Urbana-Champaign, 2021

Urbana, Illinois

Adviser:

Carolyn L. Beck

ABSTRACT

This thesis presents analysis on the epidemic processes evolving over underlying networks structures, specifically, considering an epidemic compartment model, SAIRS, that addresses the role of the asymptomatic infected subgroup of the population. Asymptomatic carriers are crucial to the epidemic spread process owning to their capacity to infect susceptible individuals, whereas it is a challenge to detect, monitor and further impose control policies on this subpopulation. This thesis first discusses the background of classic epidemics models and common converging thresholds, and then presents group SAIRS model and its networked version N-SAIRS. Equilibria and stability properties for these models are investigated. After estimating model parameters from local test-sites data with simple least-square approaches, two simulations are presented. One illustrates the effects of asymptomatic-infected individuals on the epidemic spread process with different level of control policies, the other shows the influence of different underlying network structures on the epidemic evolution in terms of networked models and the impact of local isolation on the epidemic dynamics.

ACKNOWLEDGMENTS

I grateful acknowledge funding for my education and research from Jump-ARCHES endowment through the Health Center for Engineering Systems Center (HCESC) at the University of Illinois, Urbana-Champaign, from the C3.ai Digital Transformation Institute, and from National Science Foundation (ECCS-2032321).

I would like to express profound gratitude to my advisor, Prof. Carolyn L. Beck, for her enlightenment and guidance of this work, and Dr. Joseph Kim, M.D., Ph.D., for providing informative references.

I would like to thank, most of all, my parents, who love me and support me, through all situations, and always encourage me when facing challenges.

TABLE OF CONTENTS

CHAPTER 1

INTRODUCTION

1.1 MOTIVATION

COVID-19 has become a major theme of people's lives since its first outbreak in December 2019. This epidemic, caused by Severe Acute Respiratory Syndrome CoronaVirus-2 (SARS-CoV-2), has been spreading fiercely in communities all around the world. Up until April 2021, over 134 millions of positive cases have been recorded globally, resulting in approximately 2.9 million deaths; in the United State alone, over 31 million positive cases and approximately 0.56 million deaths have resulted to date [1].

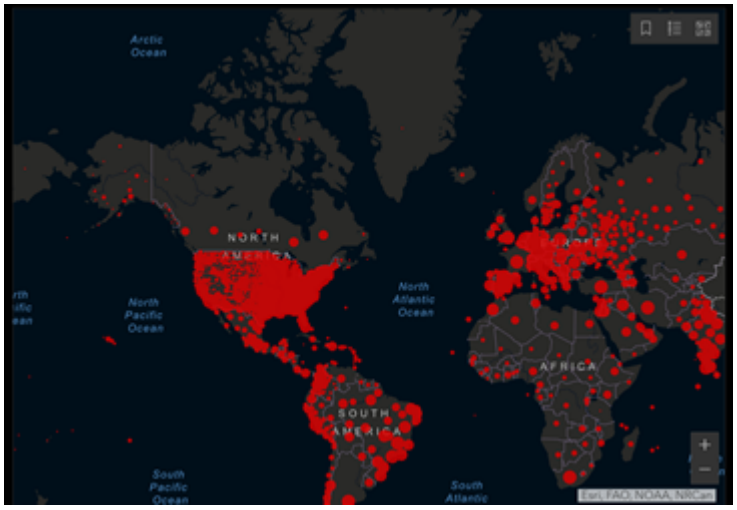

Figure 1.1: Global Cumulative COVID-19 Cases

Fighting the COVID-19 pandemic has been a challenge not only because the disease itself is highly contagious and fatal to certain subpopulations [2], but also owing to a large asymptomatic infected population [3], [4], and hence presenting the challenge to effectively detect and monitor the disease, and implement control policies. While awaiting for mitigation approaches such as vaccines to

be fully implemented, it is important to build epidemiological models for analyzing and understanding the dynamics of the epidemic. Specifically, it is crucial to capture the distinctive features of COVID-19, in particular the asymptomatic population, and to investigate the role this subgroup plays in the epidemic evolution. In this spirit, this thesis presents a compartment model structure that specifically accounts for *infectious but asymptomatic* subgroups or individuals, namely a SAIR(S) model structure, incorporating Susceptible(S), Asymptomatic-infected(A), Infected-symptomatic(I), and Recovered(R) subsets of the population. Note that the asymptomatic subset may include those individuals who do not experience symptoms through the course of their infection, as well as pre-symptomatic individuals.

1.2 BACKGROUND

Modeling, analysis and control of epidemic spread processes over networks have received increasing attention over the past decade, due to the recent COVID-19 pandemic, as well as recent outbreaks of the related SARS and MERS viruses, the Zika and Ebola viruses, and the plethora of computer network viruses. Conducting experiments to analyze infectious disease spread processes and response policies are prohibitive for many reasons, and effectively impossible over large human contact networks. As a result, mathematical modeling and simulation, informed by up-to-date data, provides an essential alternative for estimating and predicting when and how an epidemic will spread over a network. Epidemic models can be used to predict and plan for viral extent, in particular after validating the models with data collected during actual outbreaks. Moreover, simulations of strategic control policies for validated epidemic models can play an important role in quantifying the effects of mitigation strategies.

1.2.1 EPIDEMIC MODELS

Mathematical models for epidemics, or spread processes, have been proposed, analyzed and studied for over 200 years [5]. The base models for most studies today derive from the so-called *compartment models* proposed by Kermack and McKendrick in 1932 [6]. These models assume every subject lies in some segment or compartment of the population at any given time, with these compart-

ments possibly including *susceptible* (S), *infected* (I), *exposed* (E) and/or *recovered* (R) population groups, leading to the classical epidemiological models: SI (susceptible-infected), SIS (susceptible-infected-susceptible), SIR (susceptible-infected-recovered) and SEIR (susceptible-exposed-infected-recovered) models. Formulations of these classic epidemic compartmental models are presented below.

- SIS Models

Examples include the common cold (e.g., rhinoviruses), and STDs such as gonorrhea or chlamydia.

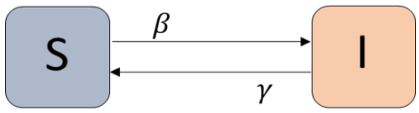

Figure 1.2: Group SIS Model

$$\begin{aligned} \dot{S}(t) &= -\beta S(t)I(t) + \delta I(t) \\ \dot{I}(t) &= \beta S(t)I(t) - \delta I(t), \end{aligned} \tag{1.1}$$

Here, $S(t)$ is the susceptible segment of the population, $I(t)$ is the infected segment of the population. β represents the transmission rate amongst infected and susceptible subgroups, and δ represents the healing or curing rate. *SI* Models are given by (1.1) with $\delta = 0$.

- SIRS Models

Examples include measles, mumps, rubella, and pertussis.

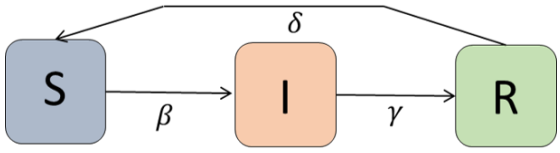

Figure 1.3: Group SIRS Model

$$\begin{aligned} \dot{S}(t) &= -\beta S(t)I(t) + \delta R(t) \\ \dot{I}(t) &= \beta S(t)I(t) - \gamma I(t) \\ \dot{R}(t) &= \gamma I(t) - \delta R(t), \end{aligned} \tag{1.2}$$

Compared to SIS (1.1) models, SIRS models (1.2) include a recovered segment of the population, $R(t)$, and model parameter γ represents the recovery rate. *SIR* Models are given by (1.2) with $\delta = 0$, and represent the situation where immunity is permanent following recovery.

- SEIRS Models

Examples include chicken pox, dengue hemorrhagic fever and HIV.

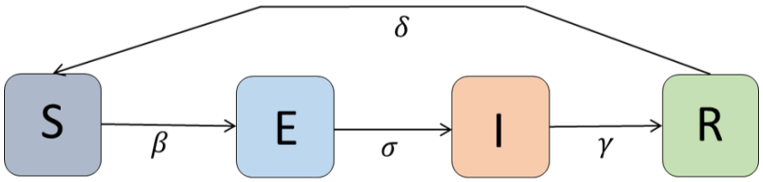

Figure 1.4: Group SEIRS Model

$$\begin{aligned} \dot{S}(t) &= -\beta S(t)I(t) + \delta R(t) \\ \dot{E}(t) &= \beta S(t)I(t) - \sigma E(t) \\ \dot{I}(t) &= \sigma E(t) - \gamma I(t) \\ \dot{R}(t) &= \gamma I(t) - \delta R(t), \end{aligned} \tag{1.3}$$

SEIRS models (1.3) capture an exposed fraction of the population, $E(t)$. A susceptible(healthy) individual becomes exposed after having contact with infected individuals, and with rate σ transitions to the infected state. The exposed segment is typically assumed to be non-infectious with the accompanying rate parameter capturing the disease incubation period. *SEIR* models are given by (1.3) with $\delta = 0$.

In Chapter 2, a new compartmental model specifcally for COVID-19, the SAIR(S) (susceptible-asymptomatic-infected-recovered) model is presented. This model was first introduced for this purpose in public online seminars and panel discussions [7],[8], and in the literature in [9]. Compartment models with different structures but including explicit asymptomatic population segments were previously proposed for dengue fever [10] and rumor spreading over online social networks [11]. Note that, despite the fact that both *SEIR* and *SAIR* models capture the feature of incubation period of the epidemic, infected individuals during their incubation period, that is compartment E in *SEIR* models and compartment A in *SAIR* models, are assumed to be infectious only in the latter model structure. Therefore, $SAIR(S)$ models are relatively more accurate to capture the evolving process of COVID-19 [12], [13].

All of the above foundational models assume: (1) a homogeneous population with no vital dynamics, meaning that infection and healing are assumed to occur at faster rates than vital dynamics (natural birth and death rates) and the population size is assumed to remain constant; and (2) the population mixes over a trivial

network, or in other words, over a complete graph structure. These assumptions have led to errors in previous epidemic forecasts [14]. To address the limits in these assumptions, and to better model spreading processes of computer viruses over communication networks, there has been an extensive study of epidemic processes evolving over complex network structures; see for example [15], [16], [17], [18], and from a controls perspective [19].

To account for network structure among members of a population, an agent-based perspective of epidemic processes is taken where each agent is represented by a node in the network, and the edges in the network between nodes represent the strength of the interaction between agents. Nodes in the network may represent either individuals or subgroups in the larger population. Given a total of n such nodes, epidemic processes can be described by large Markov process models (e.g., of dimension 2^n for SIS models and 3^n for SIR models), which capture the probability of each node transitioning from susceptible to infected, and/or to recovered states, and back. These probabilities are determined by the infection rate(s), healing rate(s) and/or recovery rate(s), in addition to the network interconnection structure, and capture the stochastic evolution of such epidemic processes. As n increases, these models quickly become intractable to analyze due to their size, at which point it has been reasoned that *mean-field approximation* (MFA) models are appropriate; these models are derived by taking expectations over infection transition rates of the agents and rely fundamentally on the work of Feller [20] and Kurtz [21].

For agents interconnected via a graph with adjacency matrix $W = [W_{ij}]$,where element W_{ij} defines the strength of the connection from node i to node j, using the assumptions of large and constant agent population size along with additional independence assumptions, the deterministic networked MFA dynamic models are now widely applied; these models have been analyzed in detail and shown to provide upper bounds on the probability of infection of a given agent at any given time (see [22] and [23] for discussions and perspectives). Considering an SIS process example, denoting the probability of node i being infected at time t by $p_i(t) \in [0,1]$, the following differential equation provides a MFA model of the evolution of the probabilities of infection of the nodes:

$$\dot{p}_i(t) = (1 - p_i(t))\beta \sum_{j=1}^{N} W_{ij} p_j(t) - \delta p_i(t). \tag{1.4}$$

This model provides a lower complexity deterministic approximation to the full

dimension Markov process model of a SIS spread process evolving over a static network. Further details can be found in [24],[19],[25]. Discrete time versions of these approximation models have also been proposed and studied in [26],[27].

1.2.2 CONVERGENCE ASSESSMENT

The primary goals in most analyses of epidemic process dynamics include computing the system equilibria, and determining the convergence behavior of these processes near the equilibria. Two kinds of equilibria are usually considered, "disease-free equilibrium" (DFE) and "endemic equilibrium". The DFE is a mathematically trivial equilibrium of the dynamics, and refers to the equlibrium where the proportions of the infected compartments of the population are zero; whereas endemic equilibria refer to fixed points where the proportions of the infected compartments are greater than zero. Taking the group *SIRS* model (1.2) as an example, equilibria are sought by setting $S(\dot{t})$, $I(\dot{t})$, and $R(\dot{t})$ to zero. When model parameter $\delta = 0$, i.e. the *SIR* model, the dynamic system has DFE at $(S^e, I^e, R^e) = (1 - c_R, 0, c_R)$, where c_R is any constant in $(0,1)$. However, when model parameter $\delta \neq 0$ and $\gamma \leq \beta$, that is the immunity an individual gains upon recovery is non-permanent and on average susceptible individuals become infected faster than infected individuals recover, the system has both a DFE at $(S^e, I^e, R^e) = (1,0,0)$ and an endemic equilibrium at $(S^e, I^e, R^e) = (\frac{\gamma}{\beta}, \frac{\delta(\beta-\gamma)}{\beta(\delta+\gamma)}, \frac{\gamma(\beta-\gamma)}{\beta(\delta+\gamma)})$.

To estimate the contagiousness of the epidemic, the "basic reproduction number", R_0, defined as the average number of secondary cases generated by a typical infected individual in a fully susceptible population, is a critical threshold quantity used widely in epidemiological studies [28],[29]. R_0 is effected by the entering and leaving influxes of the compartment states, which are further determined by the model parameters, as $R_0 = \frac{\beta}{\gamma}$ in the *SIR* (1.2) model example above, and further involves the underlying network structures in networked models. If $R_0 < 1$, the DFE of the epidemic is asymptotically stable; whereas if $R_0 > 1$, the DFE is unstable and the epidemic becomes endemic [30].

This thesis applies two approaches to derive the conditions for stability and compute R_0, the first being linearization and the eigenvalue analysis of the Jacobian matrix evaluated at the equilibrium [31], and the second incorporating the use of Lyapunov functions citekhalil. Specifically, Consider the dynamic system

$$\dot{x} = f(x), \tag{1.5}$$

where x is the state variable. With the first approach, the Jacobian matrix J_e is obtained by linearizing the state space model (1.5) and evaluating at the equilibrium point, i.e.

$$J_e = \frac{\partial f}{\partial x}|_{x=x_e}, \tag{1.6}$$

and then evaluating the eigenvalues of J_e. If J_e is Hurwitz, that is all the real-valued parts of its eigenvalues, denoted λ_i, are negative, the equilibrium point x_e is asymptotically stable. The Lyapunov function method involves finding a non-negative continuously differentiable function of the state variables, $V(x)$, such that $\dot{V(x)}$ is non-positive around the equilibrium. If $\dot{V(x)} = 0$ happens only at the equilibrium and $\dot{V(x)} < 0$ elsewhere, then the equilibrium is asymptotically stable. Under specific conditions on the Lyapunov function $V(s)$, such as radial boundedness conditions, it may be further shown that the equilibrium point is exponentially stable. Taking the networked SIS model (1.4) as an example, the DFE is globally asymptotically stable if and only if $\frac{\beta}{\delta} \leq \frac{1}{\lambda_{max}(W)}$, where $\lambda_{max}(W)$ represents the largest real-valued part of the eigenvalue of the matrix W. It has further been shown, however, that if $\frac{\beta}{\delta} > \frac{1}{\lambda_{max}(W)}$, then there exists an endemic equilibrium with $p_i^* \in (0,1)$ for all $i \in \{1,2,\ldots,n\}$ that is (almost) globally asymptotically stable, implying the system converges asymptotically to an endemic state [26],[32],[33].

Another reproduction number, namely effective reproduction number (R_{eff}) is related to R_0, and is used to assess the effect of control or mitigation strategies. In Chapter 4, the effects of asymptomatic subgroups on the epidemic spreading processes are shown by comparing the corresponding R_{eff} under different control policies.

In the remainder of the thesis, the specific SAIR(S) group and networked models are presented in Chapter 2, followed by discussion about the equilibria and stability properties of these models. Then simple parameter estimation approaches are discussed in Chapter 3, which is further applied to conduct initial model parameter estimations for the data-informed SAIRS models in Chapter 4, using local data (Champaign County Public Health District). A series of simulation studies are presented in Chapter 4 to illustrate the previously discussed stability results as well as to highlight the role the asymptomatic subgroup plays in disease spread under various quarantine policies imposed with and without awareness of asymptomatic status. Finally, the challenges as well as future directions of research are discussed in Chapter 5.

CHAPTER 2

THE SAIRS MODEL

In order to investigate the effects of asymptomatic individuals on the spread of the epidemic, we consider the effects of a proportion of the infected subgroup being asymptomatic and potentially unaware of their carrier status. Both single group models as well as networked models are evaluated, in which equilibria and stability analyses are provided.

2.1 SINGLE-GROUP AND NETWORKED MODELS

Let $S(t), A(t), I(t), R(t)$, respectively, represent the proportion of susceptible, asymptomatic-infected, symptomatic-infected, and recovered individuals at time t. The Group SAIR(S) model is characterized by

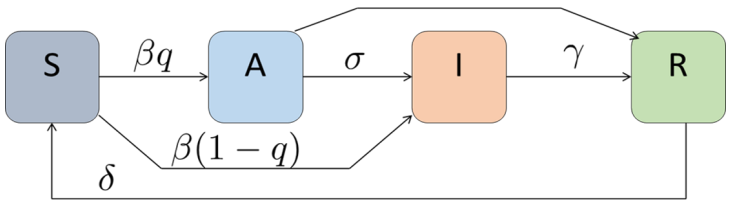

Figure 2.1: Group SAIRS Model

$$\begin{aligned}
\dot{S}(t) &= -\beta S(t)(A(t)+I(t)) + \delta R(t) \\
\dot{A}(t) &= q\beta S(t)(A(t)+I(t)) - \sigma A(t) - \kappa A(t) \\
\dot{I}(t) &= (1-q)\beta S(t)(A(t)+I(t)) + \sigma A(t) - \gamma I(t) \\
\dot{R}(t) &= \kappa A(t) + \gamma I(t) - \delta R(t).
\end{aligned} \tag{2.1}$$

Here β is the transmission rate between susceptible and infected groups, the latter of which includes both asymptomatic and symptomatic; κ and γ, respectively, are the recovery rates for asymptomatic-infected and symptomatic-infected

groups. Additionally, q captures the proportion of individuals who are asymptomatic (and/or pre-symptomatic) but still infectious; correspondingly, $(1-q)$ represents the proportion of symptomatic individuals. Further, σ is the progression rate from asymptomatic to symptomatic, and δ represents the rate at which immunity recedes. When $\delta = 0$, individuals gain permanent immunity to the infection upon recovery. These relations are assumed to hold for all $t \geq 0$.

The SAIR(S) model dynamics of n-subpopulations interconnected over an arbitrary network structure, with adjacency matrix denoted by W, is also studied. Define s_i, a_i, p_i, r_i, respectively, as the proportion of the subpopulation i that is susceptible (or healthy), asymptomatic-infected, symptomatic-infected, or recovered. The Networked SAIR(S) model (N-SAIR(S)) capturing the spread process over an arbitrary interconnection network is given by:

$$\begin{aligned}
\dot{s}_i(t) &= -\beta_i s_i(t) \textstyle\sum_j W_{ij}(a_j(t) + p_j(t)) + \delta_i r_i(t) \\
\dot{a}_i(t) &= q\beta_i s_i(t) \textstyle\sum_j W_{ij}(a_j(t) + p_j(t)) - \sigma_i a_i(t) - \kappa_i a_i(t) \\
\dot{p}_i(t) &= (1-q)\beta_i s_i(t) \textstyle\sum_j W_{ij}(a_j(t) + p_j(t)) + \sigma_i a_i(t) - \gamma_i p_i(t) \\
\dot{r}_i(t) &= \kappa_i a_i(t) + \gamma_i p_i(t) - \delta_i r_i(t),
\end{aligned} \tag{2.2}$$

where, similar to the Group Model (2.1), for a subpopulation i, β_i is the agent-to-agent transmission rate; κ_i and γ_i, respectively, are the recovery rates for asymptomatic-infected and symptomatic-infected subsets; again, σ_i represents the transition rate from asymptomatic to symptomatic infected; and δ_i represents the rate at which individuals may be susceptible to reinfection again after recovery. Since all individuals in a subgroup i will reside in one of these subsets, $s_i(t) + a_i(t) + p_i(t) + r_i(t) = 1$ holds for all i, relative to the population size, N_i of group i.

Remark: In the case where the epidemic spread is homogeneous and the underlying network topology is complete with evenly distributed interconnection weights, that is, when $W_{ij} = 1/n$ for all $i, j \in [n]$, and $(\beta_i, \kappa_i, \gamma_i, \sigma_i, \delta_i) = (\beta, \kappa, \gamma, \sigma, \delta)$ for all $i \in [n]$, the Group Model (2.1) and the Networked Model (2.2) coincide.

Prior to discussing the analysis of equilibria and stability for these models, the well-definedness of the N-SAIR(S) model is established by the following result. This result was first presented in [9] for the discrete-time case using an induction argument; it is straightforward to adapt this result to the continuous-time model given in (2.2). First, assumptions on the model parameters are stated.

Assumption 1. *For all $i, j \in [n]$, we have $\beta_i,\ \gamma_i,\ \delta_i,\ \sigma_i,\ \delta_i,\ W_{ij} \geq 0$, $0 \leq q \leq 1$.*

Lemma 1. *Consider the model in (2.2) under Assumption 1. Suppose* $s_i(0), a_i(0), p_i(0), r_i(0) \in [0,1]$, $s_i(0)+a_i(0)+p_i(0)+r_i(0)=1$ *for all* $i \in [n]$. *Then, for all* $t \geq 0$ *and* $i \in [n]$, *it holds that* $s_i(t), a_i(t), p_i(t), r_i(t) \in [0,1]$ *and* $s_i(t)+a_i(t)+p_i(t)+r_i(t)=1$.

Proof. The results are proved by showing that for all $t \geq 0$ and all $i \in [n]$, $\dot{s}_i(t) \geq 0$, $\dot{a}_i(t) \geq 0$, $\dot{p}_i(t) \geq 0$, $\dot{r}_i(t) \geq 0$ when $s_i(t)=0$, $a_i(t)=0$, $p_i(t)=0$, $r_i(t)=0$; and that $\dot{s}_i(t) \leq 0$, $\dot{a}_i(t) \leq 0$, $\dot{p}_i(t) \leq 0$, $\dot{r}_i(t) \leq 0$ when $s_i(t)=1$, $a_i(t)=1$, $p_i(t)=1$, $r_i(t)=1$.

First, since $s_i(0)+a_i(0)+p_i(0)+r_i(0)=1$, and $\dot{s}_i(t)+\dot{a}_i(t)+\dot{p}_i(t)+\dot{r}_i(t)=0$, it holds that $s_i(t)+a_i(t)+p_i(t)+r_i(t)=1, \forall i \in [n], \forall t \geq 0$.

By Assumption 1 and (2.2), for all $i \in [n]$, if $s_i(0)=0$, $\dot{s}_i(0)=\delta_i r_i(0) \geq 0$. Therefore, by the continuity of $s_i(t)$, there exist $T_{s_i} \geq 0$, such that, over the time interval $0 \leq t \leq T_{s_i}$, $s_i(t) \geq 0$. Similarly, $\dot{a}_i(0)=q\beta_i s_i(0)\sum_j W_{ij}(a_j(0)+p_j(0)) \geq 0$ if $a_i(0)=0$; $\dot{p}_i(0)=(1-q)\beta_i s_i(0)\sum_j W_{ij}(a_j(0)+p_j(0))+\sigma_i a_i(0) \geq 0$ if $p_i(0)=0$; $\dot{r}_i(0)=\kappa_i a_i(0)+\gamma_i p_i(0) \geq 0$ if $r_i(0)=0$. Thus, there exist $T_{a_i} \geq 0$, $T_{p_i} \geq 0$, $T_{r_i} \geq 0$, respectively, such that $a_i(t) \geq 0$ over the interval $0 \leq t \leq T_{a_i}$; $p_i(t) \geq 0$ over the interval $0 \leq t \leq T_{p_i}$; and $r_i(t) \geq 0$ over the time interval $0 \leq t \leq T_{r_i}$.

Define $T_i := min(T_{s_i}, T_{a_i}, T_{p_i}, T_{r_i})$ for $i \in [n]$, and let $T=\min_{i\in[n]} T_i$. Then, at time $T, s_i(T) \geq 0, a_i(T) \geq 0, p_i(T) \geq 0, r_i(T) \geq 0, \forall i \in [n]$. Similar to the proof above, $\dot{s}_i(T)=\delta_i r_i(T) \geq 0$ if $s_i(T)=0$; $\dot{a}_i(T)=q\beta_i s_i(T)\sum_j W_{ij}(a_j(T)+p_j(T)) \geq 0$ if $a_i(T)=0$; $\dot{p}_i(T)=(1-q)\beta_i s_i(T)\sum_j W_{ij}(a_j(T)+p_j(T))+\sigma_i a_i(T) \geq 0$ if $p_i(T)=0$; $\dot{r}_i(T)=\kappa_i a_i(T)+\gamma_i p_i(T) \geq 0$ if $r_i(T)=0$. Thus, for all $t \geq 0$ such that $s_i(t)=0$, $a_i(t)=0$, $p_i(t)=0$ or $r_i(t)=0$, $\dot{s}_i(t) \geq 0$, $\dot{a}_i(t) \geq 0$, $\dot{p}_i(t) \geq 0$, $\dot{r}_i(t) \geq 0$, respectively. This further suggests that, for all $i \in [n]$, $s_i(t) \geq 0$, $a_i(t) \geq 0$, $p_i(t) \geq 0$, $r_i(t) \geq 0$ for all $t \geq 0$.

The next step is to prove that $\dot{s}_i(t) \leq 0$, $\dot{a}_i(t) \leq 0$, $\dot{p}_i(t) \leq 0$, $\dot{r}_i(t) \leq 0$ when $s_i(t)=1$, $a_i(t)=1$, $p_i(t)=1$, $r_i(t)=1$, respectively. By Assumption 1, $s_i(t)+a_i(t)+p_i(t)+r_i(t)=1$, and $s_i(t), a_i(t), p_i(t), r_i(t) \geq 0, \forall i \in [n]$, when $s_i(t)=1$, we have $a_i(t)=0, p_i(t)=0, r_i(t)=0$, which leads to $\dot{s}_i(t)=-\beta_i\sum_j W_{ij}(a_j(t)+p_j(t)) \leq 0$. Similarly, $\dot{a}_i(t)=-\sigma_i-\kappa_i \leq 0$ when $a_i(t)=1$; $\dot{p}_i(t)=-\gamma_i \leq 0$ when $p_i(t)=1$; and $\dot{r}_i(t)=-\delta_i \leq 0$ when $r_i(t)=1$. Thus, it holds that $s_i(t) \leq 1$, $a_i(t) \leq 1$, $p_i(t) \leq 1$, $r_i(t) \leq 1, \forall i \in [n], \forall t \geq 0$. □

2.2 EQUILIBRIA AND STABILITY

To quantitatively and qualitatively evaluate the propagation of the virus, the corresponding basic reproduction number, R_0, of the SAIRS model is investigated. This number indicates how rapidly infected individuals transmit the virus to healthy individuals. As was discussed in Chapter 1, the condition $R_0 < 1$ needs to be satisfied in order to stop the virus from spreading exponentially. The goal of this section is to evaluate the SAIR(S) system equilibria and conduct stability analysis around the equilibria, leading to a stabilizing R_0 value. We first consider the group model.

2.2.1 GROUP MODEL SAIRS

Noting that $S(t) = 1 - A(t) - I(t) - R(t)$, the nonlinear system (2.1) can be written as:

$$\begin{aligned}
\dot{A}(t) &= q\beta(1 - A(t) - I(t) - R(t))(A(t) + I(t)) - \sigma A(t) - \kappa A(t) \\
\dot{I}(t) &= (1-q)\beta(1 - A(t) - I(t) - R(t))(A(t) + I(t)) + \sigma A(t) - \gamma I(t) \\
\dot{R}(t) &= \kappa A(t) + \gamma I(t) - \delta R(t)
\end{aligned} \tag{2.3}$$

Setting $\dot{A}(t), \dot{I}(t), \dot{R}(t)$ to 0, it is obvious that an equilibrium state of system (2.3) is given by $(A^e, I^e, R^e) = (0, 0, 0)$ with $S^e = 1$. This is the disease-free equlibrium (DFE) in the case of non-permanent immunity ($\delta \neq 0$). Linearizing system (2.3) around (A^e, I^e, R^e), the system Jacobian matrix is obtained as

$$J^e = \begin{bmatrix} q\beta - \kappa - \sigma & q\beta & 0 \\ (1-q)\beta + \sigma & (1-q)\beta - \gamma & 0 \\ \kappa & \gamma & -\delta \end{bmatrix}. \tag{2.4}$$

Applying Theorem 4.7 from [34] implies the system will be globally asymptotically stable around the DFE if all eigenvalues of J^e have negative real parts. Computing the characteristic polynomial for J^e, after some straightforward manipulations, we have

$$\det(\lambda I - J^e) = (\lambda + \delta) \cdot \left[(\lambda - q\beta + \kappa + \sigma)(\lambda - (1-q)\beta + \gamma) - q(1-q)\beta^2 - q\beta\sigma \right] \tag{2.5}$$

Applying the Routh-Hurwitz criterion from [35] to the second order polynomial in (2.5) gives the following.

Proposition 1. *For the system given by (2.3), the DFE* $(S^e, A^e, I^e, R^e) = (1,0,0,0)$ *is globally asymptotically stable (GAS) when*

$$R_0 := \max\left(\frac{\beta}{\kappa+\gamma+\sigma}, \frac{\beta(q\gamma+(1-q)\kappa+\sigma)}{\gamma(\kappa+\sigma)}\right) < 1. \tag{2.6}$$

Further, in the case where $\delta = 0$, that is when immunity following recovery from infection is permanent, the DFE (shown in Figure 2.2) will be any points $(S^e, A^e, I^e, R^e) = (c_S, 0, 0, c_R)$, where constants c_R, c_S satisfy $c_S + c_R = 1$. Analyzing the Jacobian for (2.3) in this case gives that the equilibria $(S^e, A^e, I^e, R^e) = (c_S, 0, 0, c_R)$ are globally asymptotically stable (GAS) again when (2.6) is satisfied. That is, this basic reproduction number expression provides an appropriate threshold for determining when the spread process for the SAIR(S) model will or will not spread exponentially in either of the scenarios of permanent or non-permanent immunity.

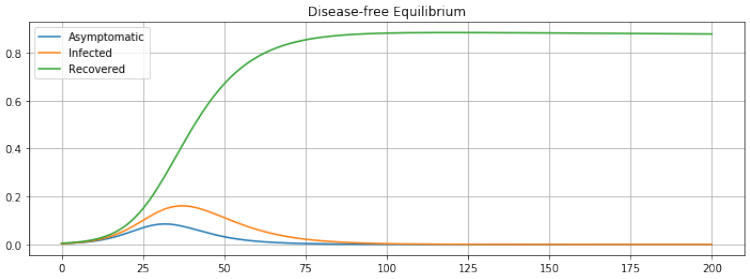

Figure 2.2: Group/Network SAIRS Simulation: DFE

Next, consider the case where the asymptomatic-infected and symptomatic-infected individuals have different infection transmission rates. In the case of COVID-19, this difference could be partly due to the inability to conduct large-scale population testing which hinders the efficient identification and isolation of asymptomatic individuals. Thus, the effectiveness of the quarantine control policies over these two subpopulations are different.

In this case, denote the infection transmission rates for agent-to-agent contact between the susceptible subgroup and the two infectious groups, respectively, as β_A, β_I. As in the preceding analysis, the Jacobian matrix around the disease-free

equilibrium $(S^e, A^e, I^e, R^e) = (1,0,0,0)$ is obtained as

$$J^e = \begin{bmatrix} q\beta_A - \kappa - \sigma & q\beta_I & 0 \\ (1-q)\beta_A + \sigma & (1-q)\beta_I - \gamma & 0 \\ \kappa & \gamma & -\delta \end{bmatrix}. \tag{2.7}$$

Following a similar approach as before yields:

$$R_0 := \max\left(\frac{q\beta_A + (1-q)\beta_I}{\kappa+\gamma+\sigma}, \frac{q\beta_A\gamma + \beta_I((1-q)\kappa+\sigma)}{\gamma(\kappa+\sigma)}\right) \tag{2.8}$$

For GAS, again it requires that $R_0 < 1$.

Discussions above illustrate the stability thresholds for the DFE under the condition $R_0 < 1$. Now consider the case with $R_0 > 1$ where an endemic equilibrium for (2.3) is investigated [36]. In this case, assume non-permanent immunity for the recovered subgroup, that is, $\delta > 0$. Setting $\dot{A}(t), \dot{I}(t), \dot{R}(t)$ to 0, the endemic equilibrium (Shown in Fig. 2.3) is obtained as

$$\begin{bmatrix} S^e \\ A^e \\ I^e \\ R^e \end{bmatrix} = \begin{bmatrix} \frac{\gamma(\kappa+\sigma)}{\beta(q\gamma+(1-q)\kappa+\sigma)} \\ \frac{q\delta\gamma\Big(\beta(q\gamma+(1-q)\kappa+\sigma)-\gamma(\kappa+\sigma)\Big)}{\beta(q\gamma+(1-q)\kappa+\sigma)\Big(\gamma(\kappa+\sigma)+\delta(q\gamma+(1-q)\kappa+\sigma)\Big)} \\ \frac{\delta((1-q)\kappa+\sigma)\Big(\beta(q\gamma+(1-q)\kappa+\sigma)-\gamma(\kappa+\sigma)\Big)}{\beta(q\gamma+(1-q)\kappa+\sigma)\Big(\gamma(\kappa+\sigma)+\delta(q\gamma+(1-q)\kappa+\sigma)\Big)} \\ \frac{\gamma(\kappa+\sigma)\Big(\beta(q\gamma+(1-q)\kappa+\sigma)-\gamma(\kappa+\sigma)\Big)}{\beta(q\gamma+(1-q)\kappa+\sigma)\Big(\gamma(\kappa+\sigma)+\delta(q\gamma+(1-q)\kappa+\sigma)\Big)} \end{bmatrix}. \tag{2.9}$$

Denoting $\Psi = \gamma(\kappa+\sigma)$ and $\Phi = q\gamma + (1-q)\kappa + \sigma$, and noting both $\Psi > 0$ and

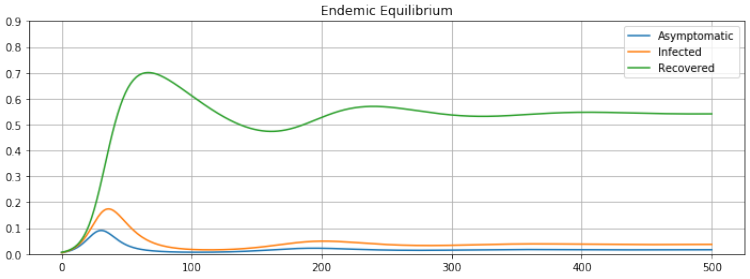

Figure 2.3: Group/Network SAIRS Simulation: Endemic Equilibrium

$\Phi > 0$, and further defining

$$C = \beta\Phi - \Psi = \beta(q\gamma + (1-q)\kappa + \sigma) - \gamma(\kappa + \sigma),$$
$$D = \delta\Phi + \Psi = \delta(q\gamma + (1-q)\kappa + \sigma) + \gamma(\kappa + \sigma) > 0,$$

then the endemic equilibrium can be written as

$$\begin{bmatrix} S^e \\ A^e \\ I^e \\ R^e \end{bmatrix} = \begin{bmatrix} \frac{\Psi}{\beta\Phi} \\ \frac{q\delta\gamma(\beta\Phi-\Psi)}{\beta\Phi(\delta\Phi+\Psi)} \\ \frac{\delta((1-q)\kappa+\sigma)(\beta\Phi-\Psi)}{\beta\Phi(\delta\Phi+\Psi)} \\ \frac{\Psi(\beta\Phi-\Psi)}{\beta\Phi(\delta\Phi+\Psi)} \end{bmatrix} = \begin{bmatrix} \frac{\Psi}{\beta\Phi} \\ \frac{q\delta\gamma C}{\beta\Phi D} \\ \frac{\delta((1-q)\kappa+\sigma)C}{\beta\Phi D} \\ \frac{\Psi C}{\beta\Phi D} \end{bmatrix}.$$

From this expression for the endemic equilibrium point, the Jacobian matrix evaluated at this equilibrium is computed as

$$J^e = \begin{bmatrix} -\frac{(\kappa+\sigma)\left((1-q)\kappa+\sigma\right)}{\Phi} - \frac{q\delta C}{D} & \frac{q\Psi}{\Phi} - \frac{q\delta C}{D} & -\frac{q\delta C}{D} \\ \frac{(\gamma+\sigma)\left((1-q)\kappa+\sigma\right)}{\Phi} - \frac{(1-q)\delta C}{D} & -\frac{q\gamma(\gamma+\sigma)}{\Phi} - \frac{(1-q)\delta C}{D} & -\frac{(1-q)\delta C}{D} \\ \kappa & \gamma & -\delta \end{bmatrix}.$$

Letting $F = \gamma + \kappa + \sigma$, following the same eigenvalue analysis discussed previously, the GAS of the endemic equilibrium requires:

$$C > 0,$$

and

$$\frac{(CD+D^2)(\delta+F)\Phi(F\Phi-\Psi) - D^2\Psi(F\Phi-\Psi) + \delta(\delta+F)(C^2+CD)\Phi^2 + \delta CD\Phi(F\Phi-\Phi^2-\Psi)}{CD\Psi\Phi^2} > 1.$$

2.2.2 NETWORKED MODEL N-SAIR(S)

The previous section discusses the equilibria and their stability properties for the group SAIR(S) models; in this section, corresponding properties for the net-

worked models N-SAIR(S) are presented. First, consider the case with permanent immunity, i.e., $\delta = 0$. Given $s_i(t) = 1 - a_i(t) - p_i(t) - r_i(t)$ for all $t \geq 0,\ i \in [n]$, system (2.2) can be represented in matrix form as

$$\begin{aligned}
\dot{a(t)} =& [q(I - A(t) - P(t) - R(t))BW - \Sigma - K]a(t) \\
&+ q(I - A(t) - P(t) - R(t))BW\,p(t) \\
\dot{p(t)} =& [(1-q)(I - A(t) - P(t) - R(t))BW + \Sigma]a(t) \\
&+ [(1-q)(I - A(t) - P(t) - R(t))BW - \Gamma]p(t) \\
\dot{r(t)} =& Ka(t) + \Gamma p(t).
\end{aligned} \tag{2.10}$$

Here,

$$a(t) = \begin{bmatrix} a_1(t) \\ \vdots \\ a_n(t) \end{bmatrix},\ p(t) = \begin{bmatrix} p_1(t) \\ \vdots \\ p_n(t) \end{bmatrix},\ r(t) = \begin{bmatrix} r_1(t) \\ \vdots \\ r_n(t) \end{bmatrix},$$

with $n \times n$ matrices $A(t) = diag(a_i(t))$, $P(t) = diag(p_i(t))$, $R(t) = diag(r_i(t))$, $B = diag(\beta_i)$, $K = diag(\kappa_i)$, $\Gamma = diag(\gamma_i)$, $\Sigma = diag(\sigma_i)$, $\Delta = diag(\delta_i)$, and adjacency matrix W.

Setting $\dot{a}(t), \dot{p}(t), \dot{r}(t)$ to 0 and computing the equilibrium state, the DFE is obtained as $(a^e, p^e, r^e) = (\overline{0}, \overline{0}, \overline{r_c})$, where $\overline{r_c}$ is any non-negative constant vector with elements $r_{c_i} < 1$. Linearizing the system (2.10) at the equilibrium (a^e, p^e, r^e), the $3n \times 3n$ system Jacobian matrix is obtained as

$$J^e = \begin{bmatrix} q(I - R_c)BW - \Sigma - K & q(I - R_c)BW & 0 \\ (1-q)(I - R_c)BW + \sigma & (1-q)(I - R_c)BW - \Gamma & 0 \\ K & \Gamma & -\Delta \end{bmatrix}. \tag{2.11}$$

Analysis of this Jacobian matrix leads to a set of constraints on the spectrum of the weighting matrix W. Alternatively, the Lyapunov function method presented in Chapter 1 is applied here to derive the stability condition.

Consider a quadratic Lyapunov function $V = a^T B^{-1} a + p^T B^{-1} p$. Computing the derivative, it is easy to show that

$$\dot{V} \leq a^T [qW - B^{-1}(\Sigma + K)]a + p^T [(1-q)W - b^{-1}\Gamma]p + a^T (W + B^{-1}\Sigma)p. \tag{2.12}$$

For GAS, $\dot{V} < 0$ is required for all $t \geq 0$, which after some algebraic manipulations

can be shown to be equivalent to the inequality

$$\begin{bmatrix} a^T & p^T \end{bmatrix} \begin{bmatrix} qW & \frac{1}{2}W \\ \frac{1}{2}W & (1-q)W \end{bmatrix} \begin{bmatrix} a \\ p \end{bmatrix} < \begin{bmatrix} a^T & p^T \end{bmatrix} \begin{bmatrix} B^{-1}(\Sigma+K) & -\frac{1}{2}B^{-1}\Sigma \\ -\frac{1}{2}B^{-1}\Sigma & B^{-1}\Gamma \end{bmatrix} \begin{bmatrix} a \\ p \end{bmatrix}. \tag{2.13}$$

Further applying the Rayleigh quotient from [35] gives the following sufficient condition for the DFE:

$$\begin{bmatrix} qW & \frac{1}{2}W \\ \frac{1}{2}W & (1-q)W \end{bmatrix} \prec \begin{bmatrix} B^{-1}(\Sigma+K) & -\frac{1}{2}B^{-1}\Sigma \\ -\frac{1}{2}B^{-1}\Sigma & B^{-1}\Gamma \end{bmatrix}, \tag{2.14}$$

where $\prec$ denotes relative definiteness of the matrices. That is, (2.14) provides a test that bounds the maximum eigenvalue of the q-scaled adjacency matrix W in terms of the minimum eigenvalue of a matrix consisting of diagonal block entries of ratios of healing and transition rates (κ_i, γ_i and σ_i) to infection rates (β_i); this loosely generalizes the usual R_0 threshold to allow for heterogeneous infection parameters over multiple infection compartments.

CHAPTER 3

PARAMETER ESTIMATION

As was noted in Chapter 1, in the simulations presented in Chapter 4, values for the N-SAIR(S) model parameters are determined based on both estimation results using local data and similarly estimated values from the literature. In this Chapter, a simple least-squares approach are presented to estimate parameter values for a discrete-time N-SAIRS model, given in (3.1). Some initial estimation results using local data for COVID-19 are further presented.

As the referencing data from Champaign County Public Health District is sampled on a daily basis, a discrete-time model would be better suited for estimating and evaluating model parameters. Thus, the first step is to apply a forward Euler's method to the continuous-time networked system (2.2), which gives a discrete-time networked SAIRS model,

$$\begin{aligned} a_i^{k+1} &= a_i^k + q\beta_i(1-a_j^k-p_j^k-r_j^k)\sum_j W_{ij}(a_j^k+p_j^k) - \sigma_i a_i^k - \kappa_i a_i^k \\ p_i^{k+1} &= p_i^k + (1-q)\beta_i(1-a_j^k-p_j^k-r_j^k)\sum_j W_{ij}(a_j^k+p_j^k) + \sigma_i a_i^k - \gamma_i p_i^k \\ r_i^{k+1} &= r_i^k + \kappa_i a_i^k + \gamma_i p_i^k - \delta_i p_i^k. \end{aligned} \tag{3.1}$$

Since the simulation update in this thesis will be daily and the sampling rate is once-per-day, the sampling parameter typically made explicit in sampled-data models will be 1 and thus is not explicitly noted above.

3.1 ASYMPTOMATIC PROPORTION ESTIMATION

Due to the difficulties in identifying and monitoring infected individuals without symptoms, explicit and unbiased information for asymptomatic-infected estimations is not always available. Applying the Next-Day Law approach proposed

by Nesterov in [37], the number of asymptomatic carriers is estimated per day, based on a latent period assumption, and the proportion q of the asymptomatic subpopulation is further estimated as a fraction of the total population. Note that this approach more accurately gives the pre-symptomatic subpopulation proportion than that of individuals who never show symptoms throughout their infection course. the Next-Day Law is included here for completeness.

Proposition 2. *[37] Let $T(d)$ represent the total number of confirmed cases by day d, and $A(d)$ represent the number of asymptomatic infected individuals at the beginning of day d. Assume the latent period (that is the time from exposure to onset of symptoms) is a constant time of Δ days. Then, $A(d+1) = T(d+\delta) - T(d), \forall d \in \mathbb{Z}$*

From the estimated daily asymptomatic population, the proportions q and $1-q$ of asymptomatic and symptomatic-infected subgroups are further estimated. Using the first two equations in (3.1), and omitting the linear terms, it is shown that

$$\frac{a_i^{k+1} - a_i^k}{p_i^{k+1} - p_i^k} \approx \frac{q}{1-q}.$$

Hence, the proportion of the asymptomatic subgroup q can be simply estimated as $\frac{a_i^{k+1}-a_i^k}{(a_i^{k+1}-a_i^k)+(p_i^{k+1}-p_i^k)}$.

3.2 LEAST SQUARES ESTIMATION OF MODEL PARAMETERS

With q known or estimated, a simple least-squares approach can be applied to estimate the model parameters $\beta_i, \sigma_i, \kappa_i, \gamma_i$, and δ_i. This approach was first outlined in [38], and further described for SAIRS models in [9]. First we rewrite the networked system (3.1) in matrix form. Let

$$b = \begin{bmatrix} a_i^1 - a_i^0 \\ \vdots \\ a_i^T - a_i^{T-1} \\ p_i^1 - p_i^0 \\ \vdots \\ p_i^T - p_i^{T-1} \\ r_i^1 - r_i^0 \\ \vdots \\ r_i^T - r_i^{T-1} \end{bmatrix}, \mathscr{A} = \begin{bmatrix} \Phi_i \\ \Sigma_i \\ \Gamma_i \end{bmatrix}, x = \begin{bmatrix} \beta_i \\ \sigma_i \\ \gamma_i \\ \kappa_i \\ \delta_i \end{bmatrix}, \tag{3.2}$$

with

$$\Phi_i = \begin{bmatrix} qs_i^0 \sum_j W_{ij}(a_j^0 + p_j^0) & -a_i^0 & 0 & -a_i^0 & 0 \\ \vdots & \vdots & \vdots & \vdots & \vdots \\ qs_i^{T-1} \sum_j W_{ij}(a_j^{T-1} + p_j^{T-1}) & -a_i^{T-1} & 0 & -a_i^{T-1} & 0 \end{bmatrix},$$

$$\Sigma_i = \begin{bmatrix} (1-q)s_i^0 \sum_j W_{ij}(a_j^0 + p_j^0) & a_i^0 & -p_i^0 & 0 & 0 \\ \vdots & \vdots & \vdots & \vdots & \vdots \\ (1-q)s_i^{T-1} \sum_j W_{ij}(a_j^{T-1} + p_j^{T-1}) & a_i^{T-1} & -p_i^{T-1} & 0 & 0 \end{bmatrix},$$

$$\Gamma_i = \begin{bmatrix} 0 & 0 & a_i^0 & p_i^0 & -r_i^0 \\ \vdots & \vdots & \vdots & \vdots & \vdots \\ 0 & 0 & a_i^{T-1} & p_i^{T-1} & -r_i^{T-1}, \end{bmatrix}$$

where $s_i^k = 1 - a_i^k - p_i^k - r_i^k, \forall i \in [n], k \in \mathbb{Z}$.

Then the discrete-time networked SAIRS model can be written in the form of a system of linear equations,

$$b = \mathscr{A} x \qquad \forall i \in [n] \tag{3.3}$$

That is, since q is assumed known, (3.3) is linear with respect to the remaining model parameters. When $\mathscr{A}$ is full rank, the parameters $\beta_i^*, \sigma_i^*, \gamma_i^*, \kappa_i^*$, and δ_i^* can be recovered using the pseudo-inverse in the least-squares solution (3.3).

3.3 PRELIMINARY ESTIMATION RESULTS

Based on local COVID-19 testing-site data from Champaign County, Illinois, dating from May to September, this section presents initial parameter estimations for different phases of the state restoration plans, which were scheduled as:

$$\begin{aligned}
&\textit{Phase } 1 : \textit{Rapid Spread } (04/01/2020 - 05/01/2020)\\
&\textit{Phase } 2 : \textit{Flattening } (05/01/2020 - 05/29/2020)\\
&\textit{Phase } 3 : \textit{Recovery } (05/29/2020 - 06/26/2020)\\
&\textit{Phase } 4 : \textit{Revitalization } (06/26/2020 - 09/26/2020)
\end{aligned}$$

Assume a latent period of $\Delta = 6$ days.
The estimation results are given here:

Phases	q	β	σ	γ	κ	R_0
Phase 2	0.7	0.06	0.22	0.15	-0.10	1.004
Phase 3	0.6	0.07	0.15	0.15	-0.05	1.156
Phase 4	0.6	0.07	0.08	0.11	0.02	1.104

It is noted from these estimation results, as the epidemic progresses, the basic reproduction number R_0 first rises, and then decreases with the implementation of consistent quarantine and other social distancing measures.

The preliminary results also expose problems with real data based estimation and analysis. For example, due to the reduced availability of tests and test-sites in the early stage of the epidemic, as well as a non-random sample, the testing population presented in the data is severely skewed toward Symptomatic-Infected individuals. This hinders the accurate capture of the true proportion of the Asymptomatic-Infected subgroup, as well as an accurate prevalence rate of infection over the total population.

In addition, the assumption of a constant latent period is not consistent with the nature of COVID-19; the latent period value used above is an average value [39],[40]. These issues lead to estimation errors, including the negative recovery rate values for κ in Phase 2 and Phase 3.

CHAPTER 4

SIMULATIONS

In this section, simulations of data-informed SAIRS models are presented to illustrate the role of the asymptomatic subgroup in the development of the epidemic, and to investigate the effects of quarantine and other social distancing policies. Simulations of endemic equilibria are also presented to verify the stability threshold discussed in Chapter 2.

First, to provide a baseline for more complex simulations in this section, a five-subpopulation group/networked model (2.2) simulation is presented, for which the model parameters are assumed to be homogeneous. Assume the total population size is $10,000$ and the respective subpopulations denoted A, B, C, D, and E have populations $2000, 2500, 1500, 3500$, and 500, respectively. Assume the cities are fully connected with evenly distributed edge weights, thus this baseline model is equivalent to a single group model. The corresponding adjacency matrix is

$$W = \begin{bmatrix} 0.2 & 0.2 & 0.2 & 0.2 & 0.2 \\ 0.2 & 0.2 & 0.2 & 0.2 & 0.2 \\ 0.2 & 0.2 & 0.2 & 0.2 & 0.2 \\ 0.2 & 0.2 & 0.2 & 0.2 & 0.2 \\ 0.2 & 0.2 & 0.2 & 0.2 & 0.2 \end{bmatrix} \tag{4.1}$$

the parameter values are selected using the estimation results from local data (discussed in Section 3) in addition to drawing upon the literature (e.g.,[39] [40]) on COVID-19.

$$(q, \beta, \sigma, \gamma, \kappa, \delta) = (0.7, 0.25, 0.15, 0.11, 0.08, 0.0001) \tag{4.2}$$

Furthermore, set the initial proportions of the A, I, R compartments as

$$a(0) = (a_A(0), a_B(0), a_C(0), a_D(0), a_E(0)) = (0.006, 0.004, 0.012, 0.004, 0.004)$$
$$p(0) = (p_A(0), p_B(0), p_C(0), p_D(0), p_E(0)) = (0.005, 0.002, 0.008, 0.003, 0.002)$$
$$r(0) = (r_A(0), r_B(0), r_C(0), r_D(0), r_E(0)) = (0.007, 0.003, 0.010, 0.008, 0.005)$$

Simulating the SAIRS model over 60 days, the results for the epidemic progression is shown in Fig.4.1:

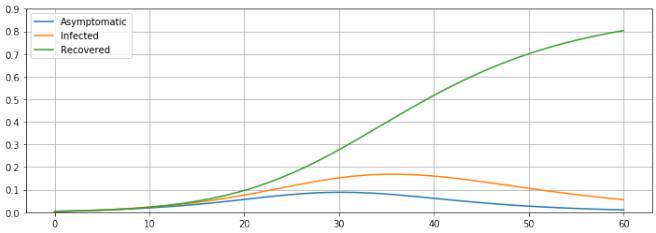

Figure 4.1: Group/Network SAIRS Simulation: Baseline Model

Note that peak active infection occurs on day 33, that is $p(t) + a(t)$ attains a maximum of approximately 28% on day $t = 33$. By day 60, approximately 87% of the entire population has been or is infected. Assume a mortality rate of 4%, this corresponds to 348 deaths in the two month time span. Again, note this model assumes homogeneous mixing within the entire population.

4.1 ASYMPTOMATIC EFFECTS

One major obstacle in the control of COVID-19 is the challenge of identifying and monitoring individuals in the asymptomatic-infected subgroup. Herein this section explores the impact of the asymptomatic subgroup on the epidemic evolution.

First, assume there is no control imposed on either the asymptomatic or symptomatic infected subgroups. For simplicity, consider the baseline model (Shown in Figure 4.1), and set initial proportions for the A, I, R compartments for each subpopulation as

$$(a(0), I(0), R(0)) = (0.004, 0.002, 0.003),$$

the simulation results is obtained as Fig. 4.2.

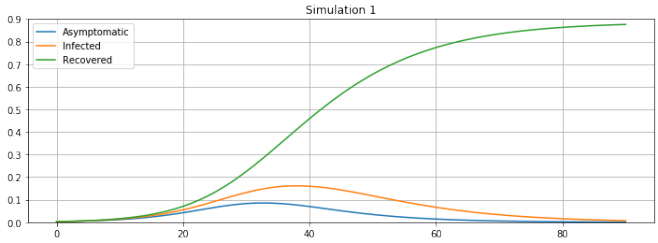

Figure 4.2: No control policies in effect on either Asymptomatic or Symptomatic Infected subgroups

The population reaches a peak infection level of approximately 25% on day 35. By day 80, approximately 87% of the population has been or is infected. From the perspective of reproduction number, this model gives a $R_0 \approx 2.5$ from (2.6).

Next, consider the case where moderate and stringent isolation policies are implemented on only the symptomatic subgroup; this is effected in the simulations by changing the respective infection rate parameters of the subgroups, which are now denoted individually by β_A and β_I. Imposing isolation policies on a subgroup effectively lowers the corresponding infection rate. The simulations results are shown in Fig. 4.3, 4.4.

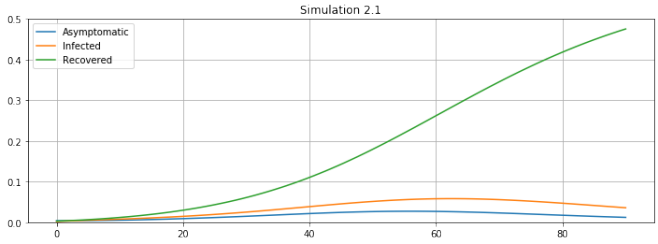

Figure 4.3: Moderate isolation of the Symptomatic Infected subgroup; $\beta_A = 0.25, \beta_I = 0.11$ giving $R_{eff} = 1.5$

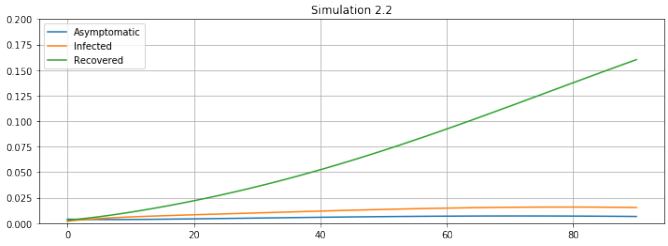

Figure 4.4: Stringent isolation of the Symptomatic Infected subgroup; $\beta_A = 0.25, \beta_I = 0.06$ giving $R_{eff} = 1.2$

Note that with isolation measures on only the symptomatic infected subgroup, the epidemic now progresses more slowly and mildly, as is expected, however there is

still substantial infection in the population. The infection peaks at days 60 and 75, respectively, approximately $4-6$ weeks later than with no control. With moderate isolation policies in effect on the I subgroup, the peak infection level is approximately 9%; and with strict isolation policies, the peak infection level attained is approximately 2.5%. Finally by day 80, the total percentages of the population that has been or is infected is approximately 49% and 17%; with a mortality rate of 4% this corresponds to 196 and 68 deaths, respectively.

Alternatively, consider the situation where Asymptomatic individuals are also identified and isolated, under both moderate and stringent policies, with the results shown in Fig 4.5, 4.6.

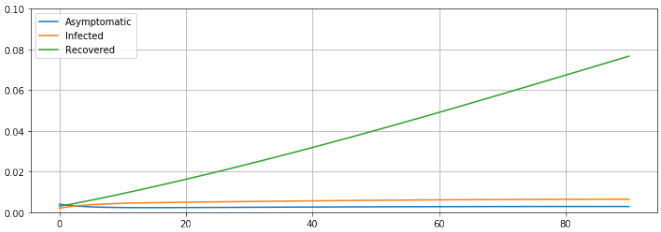

Figure 4.5: Moderate isolation of both Symptomatic and Asymptomatic Infected subgroups; $\beta_A = 0.11, \beta_I = 0.11$ giving $R_{eff} = 1.09$

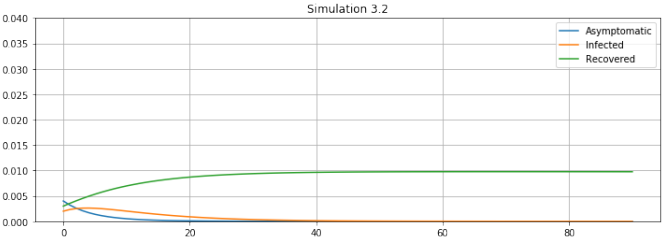

Figure 4.6: Stringent isolation of both Symptomatic and Asymptomatic Infected subgroups; $\beta_A = 0.0125, \beta_I = 0.0125$ giving $R_{eff} = 0.12$

Note that with only moderate isolation on both Asymptomatic and Symptomatic Infected groups (Figure 4.5), the epidemic is under control within three months. By day 80, approximately 7.7% of the population has been or is infected, corresponding to a total of 770 individuals in a population base of $10,000$ that have been infected; at a 4% mortality rate this corresponds to approximately 31 deaths as compared to approximately 68 deaths with stringent control imposed on only the Symptomatic Infected group (Figure 4.4).

An additional perspective to consider is the effective reproduction number under the different isolation policies. Moderate isolation of both Asymptomatic and

Symptomatic subgroups (Figure4.5) gives a $R_{eff} \approx 1.09$, while stringent isolation on just the Symptomatic subgroup (Figure 4.4) gives a $R_{eff} \approx 1.2$.

These simulation results indicate that identification and isolation of Asymptomatic infected individuals is much more effective in curbing the spread of the epidemic than identification and isolation of just the Symptomatic subgroup. However, due to the voluntary nature of most testing regimens in the United States, this type of basic control has not been implemented. To achieve this goal, either regular extensive mandatory testing policies, or persistent extensive isolation of the whole population is required.

4.2 NETWORK EFFECTS

In this section, the effects a more realistic interaction structure has on epidemic spread over a population are evaluated. Consider the 5-node baseline model (Figure 4.1), and then consider the removal of some edges between nodes.

First consider an interconnection network structure with adjacency matrix

$$W = \begin{bmatrix} \frac{1}{3} & \frac{1}{3} & \frac{1}{3} & 0 & 0 \\ \frac{1}{3} & \frac{1}{3} & 0 & 0 & \frac{1}{3} \\ \frac{1}{3} & 0 & \frac{1}{3} & \frac{1}{3} & 0 \\ 0 & 0 & \frac{1}{2} & \frac{1}{2} & 0 \\ 0 & \frac{1}{2} & 0 & 0 & \frac{1}{2} \end{bmatrix}. \tag{4.3}$$

Using the same parameters and initial conditions as used in the baseline model, the simulations return results for subpopulations C and E as shown in Fig.4.7, 4.8.

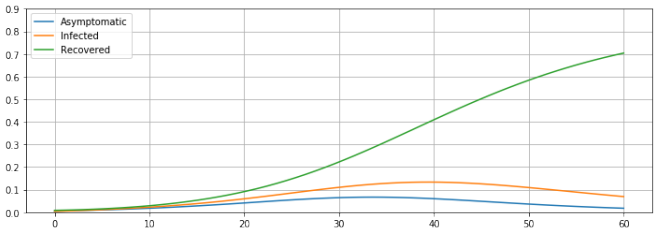

Figure 4.7: Subpopulation C

With a less strongly connected network, the epidemic spreads more slowly and weakly. Subpopulation C reaches its peak infection level at day 37, and subpopulation E at day 39. By day 60, approximately 83% of city C population and 81%

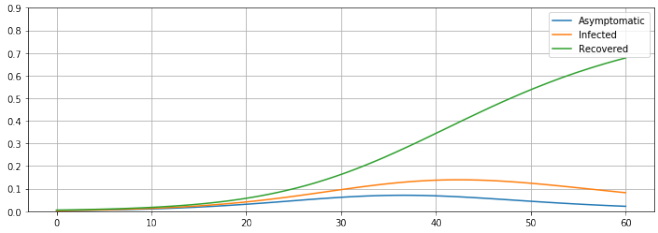

Figure 4.8: Subpopulation E

city E population have been infected. However, in total, approximately 480 fewer individuals over the five cities are infected as compared to the fully connected (i.e., complete) baseline model.

Next, to explore the impact of quarantine and stronger social distancing measures, the full population is further broken into 50 smaller subpopulations, generating stochastic adjacency matrix with each node only connected to (randomly selected) 20 nodes out of the total of 50 group nodes. We generate the initial conditions randomly, i.e., $a(0), p(0), r(0)$, assuming $a_i(0) \sim \mathcal{N}(0.04, 0.005)$, $p_i(0) \sim \mathcal{N}(0.02, 0.005)$, $r_i(0) \sim \mathcal{N}(0.03, 0.005)$, with these values restricted to be non-negative. Randomly selecting 6 of the 50 sub-populations, the simulation results as shown in Figure. 4.9:

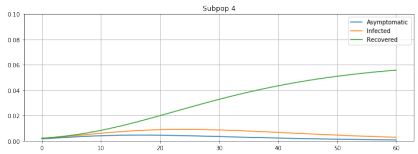

(a) Subpopulation 4

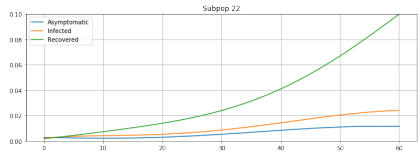

(b) Subpopulation 22

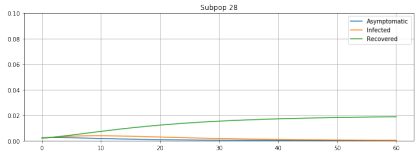

(c) Subpopulation 28

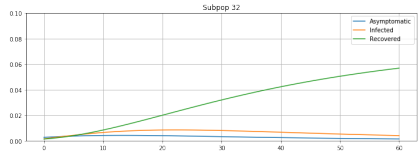

(d) Subpopulation 32

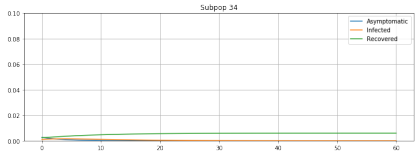

(e) Subpopulation 34

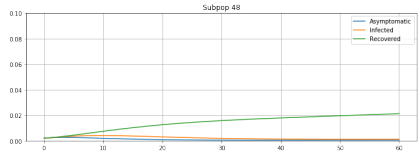

(f) Subpopulation 48

Figure 4.9: Weakly Connected Network Simulation Results

Note that, with this more extensive isolation, the epidemic decays much faster

than under the previous strongly connected network (Figure 4.7, 4.8). Subpopulations $4, 22, 28, 32, 34$ and 48, respectively, reach their peak infection levels at days $21, 59, 7, 24, 0$ and day 8. Among the six subpopulations in the sample, subpopulation 22 is the most highly infected group. However, overall after 60 days, approximately only 13.6% of the population has been or is infected, which is a reduction of 73.4% of the population compared to the fully connected network (Figure 4.1), and a reduction of 67.7% compared to the strongly connected network (Figure 4.7, 4.8). These simulations demonstrate that social distancing measures, such as quarantining within each community or family, does serve to control the spread of the epidemic, as has been seen in practice in many communities. From the perspective of the group model, extensive isolation policies help reduce the group transmission rate for person-to-person contact, which results in both faster flattening of the infection curve and fewer infected individuals (asymptomatic and symptomatic) in the whole population.

4.3 ENDEMIC EQUILIBRIA

As discussed in Section 2, the endemic equilibrium, which is GAS, is given by,

$$C = \beta(q\gamma + (1-q)\kappa + \sigma) - \gamma(\kappa + \sigma) > 0, \tag{4.4}$$

and

$$\frac{(CD+D^2)(\delta+F)\Phi(F\Phi-\Psi) - D^2\Psi(F\Phi-\Psi) + \delta(\delta+F)(C^2+CD)\Phi^2 + \delta CD\Phi(F\Phi-\Phi^2-\Psi)}{CD\Psi\Phi^2} > 1. \tag{4.5}$$

Note that the condition $C > 0$ for the existence of endemic equilibrium is equivalent to the condition for the DFE that $R_0 > 1$, therefore, as shown in the baseline model, the endemic equilibrium does not exist.

Let R_{end} denote the expression in (4.5), it can be observed that, with values for all other parameters unchanged, R_{end} increases monotonically as the value for model parameter δ increases.

Setting the initial conditions as in the baseline model, excepting a change in the parameter value of δ, simulation results of endemic equilibria with different R_{end} are presented in Figure 4.10, 4.11, 4.12.

Note that as value for R_{end} increases, the turbulence before reaching the endemic equilibrium has higher frequency but smaller amplitude. For the models

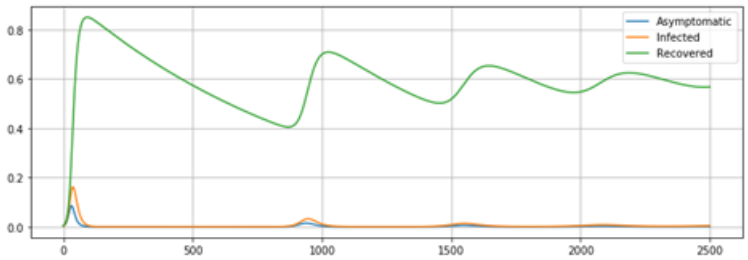

Figure 4.10: Endemic Equilibrium: $\delta = 0.001$

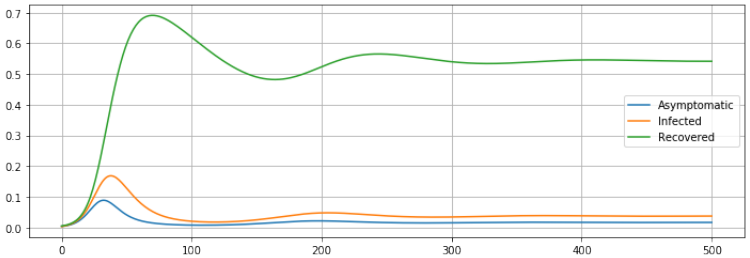

Figure 4.11: Endemic Equilibrium: $\delta = 0.01$

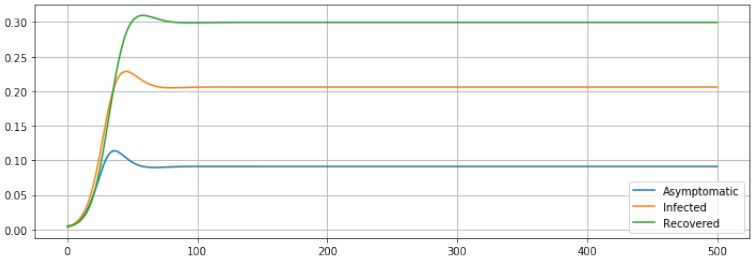

Figure 4.12: Endemic Equilibrium: $\delta = 0.1$

with parameters $\delta = 0.001$, $\delta = 0.01$, $\delta = 0.1$, the first turbulence in R subgroup takes approximately 850 days, 160 days and 55 days, respectively, and with amplitude, that is the difference in the proportion of the recovered subgroup between the first peak to the following lowest point, approximately 0.45, 0.22, 0.015, respectively. Comparing the values for the endemic equilibria points in these three models, as the value for δ increases, the value for R decreases, whereas values for A and I increase. This observation coincides with the expression of endemic equilibria presented in Chapter 2.

CHAPTER 5

DISCUSSION AND CONCLUSION

This thesis reviewed classical epidemiological compartment models, with a focus on a new SAIR(S) model that emphasizes the role of the asymptomatic-infected subpopulation. It presented continuous-time, discrete-time, and networked versions of the SAIR(S) model, and discussed their equilibria and corresponding stability properties. The thesis noted the use of Nesterov's Next-Day Law and a basic least-squares approach for model parameter estimation, and conducted initial parameter estimation for COVID-19 using publicly available data from Champaign County, Illinois. Furthermore, it presented simulations of both group and networked models, investigated the impact of isolating subpopulations, and highlighted the crucial role of the asymptomatic subgroup in the control of epidemic evolution.

In the estimation process, many challenges are met, mostly owning to the significantly biased testing data and the lack of explicit information on the asymptomatic infected population. Possible approaches to improve the situation include investigating approaches for model estimation under non-random and missing sample data sets, for example as described in [41]. This thesis also assists further investigation of Bayesian statistical methods for estimating true prevalence of epidemics under biased information on apparent prevalence.

REFERENCES

[1] J. H. University and Medicine, "Covid-19 dashboard," 2021, accessed 9 April 2021. [Online]. Available: https://coronavirus.jhu.edu/map.html

[2] E. A. Undurraga, G. Chowell, and K. Mizumoto, "Covid-19 case fatality risk by age and gender in a high testing setting in latin america: Chile, march–august 2020," *Infectious Diseases of Poverty*, 2021.

[3] H. Nishiura, T. Kobayashi, T. Miyama, A. Suzuki, S. Jung, K. Hayashi, R. Kinoshita, Y. Yang, B. Yuan, A. Akhmetzhanov, and N. Linton, "Estimation of the asymptomatic ratio of novel coronavirus infections (covid-19)," *International Journal of Infectious Diseases*, 2020.

[4] N. Furukawa, J. T. Brooks, and J. Sobel, "Evidence supporting transmission of severe acute respiratory syndrome coronavirus 2 while presymptomatic or asymptomatic," *Emerging Infectious Diseases*, vol. 26, 2020.

[5] D. Bernoulli, "Essai d'une nouvelle analyse de la mortalité causée par la petite vérole et des avantages de l'inoculation pour la prévenir," *Histoire de l'Acad. Roy. Sci. avec Mém. des Math. et Phys. and Mém*, pp. 1–45, 1760.

[6] W. O. Kermack and A. G. McKendrick, "Contributions to the mathematical theory of epidemics. II. The problem of endemicity," *Proceedings of the Royal Society A*, vol. 138, no. 834, pp. 55–83, 1932.

[7] C. L. Beck, "Accounting for network structure and dynamics in epidemic models," in *Health Care Engineering Systems Center UIUC, COVID-19 Virtual Summit*, 2020, April.

[8] C. L. Beck, "Epidemic processes and network structure," in *First Call to Arms Workshop, NSF NeTs Community and the Ohio State University*, 2020, April.

[9] P. Pare, C. Beck, and T. Başar, "Modeling, estimation, and analysis of epidemics over networks: An overview," *Annual Reviews in Control*, 2020, accepted.

[10] M. Grunnill, "An exploration of the role of asymptomatic infections in the epidemiology of dengue viruses through susceptible, asymptomatic, infected and recovered (SAIR) models," *Journal of Theoretical Biology*, vol. 439, pp. 195–204, 2018.

[11] B. W. L. Zhu, "Stability analysis of a sair rumor spreading model with control strategies in online social networks," *Information Science*, vol. 526, 2020.

[12] e. a. M. M. Arons, "Presymptomatic sars-cov-2 infections and transmission in a skilled nursing facility," *The New England Journal of Medicine*, 2020.

[13] M. Chen, P. Fan, Z. Liu, R. Pan, S. Huang, J. Li, and D. Zhao, "Presymptomatic sars-cov-2 infections and transmission in a skilled nursing facility," *Journal of Infection and Public Health*, 2020.

[14] S. Scarpino and G. Petri, "On the predictability of infectious disease outbreaks," *Nature communications*, vol. 10, 2019.

[15] J. O. Kephart and S. R. White, "Directed-graph epidemiological models of computer viruses," in *IEEE Symposium on Security and Privacy*, 1991, pp. 343–361.

[16] D. T. A. Ganesh, L. Massouli, "The effect of network topology on the spread of epidemics," in *24th Annual Joint Conference of the IEEE Computer and Communications Societies*, vol. 2, 2005, pp. 1455–1466.

[17] M. Draief and L. Massoulie', *Epidemics and rumours in complex networks*. Cambridge University Press, 2010.

[18] R. Pastor-Satorras, C. Castellano, P. Van Mieghem, and A. Vespignani, "Epidemic processes in complex networks," *Reviews of Modern Physics*, vol. 87, no. 3, p. 925, 2015.

[19] C. Nowzari, V. M. Preciado, and G. J. Pappas, "Analysis and control of epidemics: A survey of spreading processes on complex networks," *IEEE Control Systems Magazine*, no. 1, pp. 26–46, 2016.

[20] W. Feller, "On the integro-differential equations of purely discontinuous markoff processes," *Transactions of the American Mathematical Society*, vol. 48, no. 3, pp. 488–515, 1940.

[21] T. G. Kurtz, "The central limit theorem for Markov chains," *The Annals of Probability*, vol. 9, no. 4, pp. 557–560, 1981.

[22] P. V. Mieghem, J. Omic, and R. Kooij, "Virus spread in networks," *IEEE/ACM Transactions on Networking*, no. 1, pp. 62–68, 2009.

[23] S. Chatterjee and R. Durrett, "Contact processes on random graphs with power law degree distributions have critical value 0," *The Annals of Probability*, no. 6, pp. 2332–2356, 2009.

[24] A. Fall, A. Iggidr, G. Sallet, and J. J. Tewa, "Epidemiological models and Lyapunov functions," *Mathematical Modelling of Natural Phenomena*, vol. 2, no. 1, pp. 62–83, 2007.

[25] P. E. Paré, C. L. Beck, and A. Nedić, "Epidemic processes over time-varying networks," *IEEE Transactions on Control over Network Systems*, no. 3, pp. 1322–1334, 2018.

[26] H. J. Ahn and B. Hassibi, "Global dynamics of epidemic spread over complex networks," in *Proceedings of the IEEE Conference on Decision and Control*, 2013, pp. 4579–4585.

[27] Y. Wang, D. Chakrabarti, C. Wang, and C. Faloutsos, "Epidemic spreading in real networks: an eigenvalue viewpoint," in *Proceedings of the 22nd International Symposium on Reliable Distributed Systems*, 2003, pp. 25–34.

[28] P. van den Driessche, "Reproduction numbers of infectious disease models," *Infectious Disease Modelling*, vol. 2, pp. 288–303, 2017.

[29] A. Perasso, "An introduction to the basic reproduction number in mathematical epidemiology," *ESAIM: PROCEEDINGS AND SURVEYS*, vol. 62, 2018.

[30] F. Brauer, C. Castillo-Chavez, and Z. Feng, "Endemic disease models," *Nature Public Health Emergency Collection*, vol. 69, 2019.

[31] R. Morgan, "Linearization and stability analysis of nonlinear problems," *Rose-Hulman Undergraduate Mathematics Journal*, vol. 16, 2015.

[32] A. Khanafer, T. Başar, and B. Gharesifard, "Stability properties of infected networks with low curing rates," in *Proceedings of the American Control Conference*, 2014, pp. 3579–3584.

[33] A. Khanafer, T. Başar, and B. Gharesifard, "Stability properties of infection diffusion dynamics over directed networks," in *Proceedings of the IEEE Conference on Decision and Control*, 2014, pp. 6215–6220.

[34] H. K. Khalil, *Nonlinear Systems*. Prentice Hall, 2002.

[35] R. A. Horn and C. R. Johnson, *Matrix Analysis*. Cambridge University Press, 2013.

[36] X. Bi and C. L. Beck, "On the role of asymptomatic carriers in epidemic spread processes," *Preprint*, 2021, https://arxiv.org/pdf/2103.11411.pdf.

[37] Y. Nesterov, "Online prediction of covid19 dynamics.belgian case study," *Preprint*, 2020, https://arxiv.org/pdf/2007.11429.pdf.

[38] P. E. Paré, J. Liu, C. L. Beck, B. E. Kirwan, and T. Başar, "Analysis, identification, and validation of discrete-time epidemic processes," *IEEE Transactions on Control Systems Technology*, vol. 28, no. 1, pp. 79–93, 2019.

[39] S. A. Lauer, K. H. Grantz, Q. Bi, M. Q. Z. F. K. Jones, H. R. Meredith, A. S. Azman, N. G. Reich, and J. Lessler, "The incubation period of coronavirus disease 2019 (covid-19) from publicly reported confirmed cases: Estimation and application," *Annals of Internal Medicine*, 2020. [Online]. Available: https://www.acpjournals.org/doi/10.7326/M20-0504

[40] D. P. Oran and M. E. J. Topol, "Prevalence of asymptomatic sars-cov-2 infection; a narrative review," *Annals of Internal Medicine*, 2020. [Online]. Available: https://www.acpjournals.org/doi/10.7326/M20-3012

[41] J. Copas and H. Li, "Inference for non-random samples," *Journal of the Royal Statistical Society*, vol. 59, no. 1, pp. 55–95, 1997.